Supplement of Atmos. Chem. Phys., 20, 4999–5017, 2020
https://doi.org/10.5194/acp-20-4999-2020-supplement

Atmospheric Chemistry and Physics
Open Access
EGU

Supplement of

Atmospheric teleconnection processes linking winter air stagnation and haze extremes in China with regional Arctic sea ice decline

Yufei Zou et al.

Correspondence to: Yufei Zou (yufei.zou@pnnl.gov) and Yuhang Wang (yuhang.wang@eas.gatech.edu)

Supplement

Table S1-S5

Figure S1-S10

Reference

Table S1. The 8 CMIP6 models used in this study

Model Name	Modeling Center	Institute ID	Experiment ID	Ensemble Member
CAMS-CSM1-0	Chinese Academy of Meteorological Sciences	CAMS	Historical (Rong, 2019a) +ssp585 (Rong, 2019b)	r1i1p1f1
CESM2	National Center for Atmospheric Research	NCAR	Historical (Danabasoglu et al., 2019) +ssp585 (Danabasoglu, 2019a)	r1i1p1f1
CESM2-WACCM	National Center for Atmospheric Research	NCAR	Historical (Danabasoglu, 2019b) +ssp585 (Danabasoglu, 2019c)	r1i1p1f1
CanESM5	Canadian Centre for Climate Modeling and Analysis	CCCma	Historical (CCCma, 2019a) +ssp585 (CCCma, 2019b)	r1i1p1f1
EC-Earth3	The European EC-Earth consortium	EC-Earth-Consortium	Historical (EC-Earth, 2019a) +ssp585 (EC-Earth, 2019b)	r1i1p1f1
GFDL-CM4	National Oceanic and Atmospheric Administration, Geophysical Fluid Dynamics Laboratory	NOAA-GFDL	Historical (Guo et al., 2018a) +ssp585 (Guo et al., 2018b)	r1i1p1f1
IPSL-CM6A-LR	Institute Pierre-Simon Laplace	IPSL	Historical (Boucher, et al., 2018) +ssp585 (Boucher, et al., 2019)	r1i1p1f1

MIROC6	JAMSTEC, AORI, NIES, and R-CCS	MIROC	Historical (Tatebe and Watanabe, 2018) +ssp585 (Shiogama, et al., 2019)	r1i1p1f1

6

Table S2. The statistical properties of the MCA_Z500 and ECP_PPI indices in the WACCM experiments

	CTRL		SENSall		SENSr1		SENSr2		SENSr3	
Variables	Z500	PPI	Z500	PPI	Z500	PPI	Z500	PPI	Z500	PPI
Mean	0.0	0.0	0.01	-0.06	-0.07	-0.13	0.01	0.03	0.01	-0.02
Std	0.50	0.44	0.54	0.49	0.51	0.43	0.54	0.54	0.53	0.46
Skewness	0.17	-0.13	-0.66	-0.18	-0.13	0.24	0.73	0.56	-0.39	-0.32
Kurtosis	0.07	-0.78	0.27	0.55	-0.04	-0.52	0.48	-0.38	-0.35	-0.31
p-value[(a)]	0.51	0.21	0.01	0.21	1.00	0.39	0.01	0.01	0.13	0.17
p-value[(b)]	–	–	0.90	0.43	0.30	0.04	0.87	0.61	0.95	0.72

[(a)]: p values of the Shapiro-Wilk normality test;

[(b)]: p values of the two-sided Student's t-test for the ensemble mean comparison of the two-paired samples from CTRL and SENS experiments;

Table S3. The bootstrap (nboot=10000) estimates (ensemble mean and 95% percentile range) of positive extreme probabilities of the MCA_Z500 and ECP_PPI indices in the WACCM experiments

	CTRL	SENSall	SENSr1	SENSr2	SENSr3
MCA_Z500	5.0%	3.7% (0-13.5%)	3.3% (0-9.2%)	7.5% (0.8-16.4%)	4.1% (0-12.8%)
ECP_PPI	5.0%	7.0% (0.7-16.1%)	4.1% (0.4-9.2%)	11.6% (5.2-18.4%)	5.0% (0.2-11.0%)

Table S4. The bootstrap (nboot=10000) estimates (ensemble mean and 95% percentile range) of positive extreme intensities of the MCA_Z500 and ECP_PPI indices in the WACCM experiments

	CTRL	SENSall	SENSr1	SENSr2	SENSr3
MCA_Z500	1.14 (0.75-1.72)	1.00 (0.77-1.35)	1.07 (0.81-1.44)	1.27 (0.90-1.68)	1.03 (0.77-1.41)
ECP_PPI	0.86 (0.63-1.40)	0.91 (0.70-1.25)	0.94 (0.72-1.31)	1.12 (0.90-1.42)	0.84 (0.66-1.13)

Table S5. Changes in ensemble mean values and probabilities of positive extreme values of ECP_PPI in the CMIP6 models

	Time	NCEP	CAMS-CSM1-0	CESM2	CESM2-WACCM	CanESM5	EC-Earth3	GFDL-CM4	IPSL-CM6A-LR	MIROC6
Mean	P1	-0.38	-0.36	-0.07	0.03	-0.02	-0.27	0.06	0.12	0.12
	P2	0.30	-0.16	0.20	0.36	0.10	-0.21	0.14	0.08	0.02
	P3	-	-0.23	0.11	0.27	0.22	-0.25	0.26	0.30	0.00
$P_{extreme}$	P1	5%	5%	5%	5%	5%	5%	5%	5%	5%
	P2	19%	11%	11%	10%	7%	5%	6%	7%	2%
	P3	-	13%	13%	6%	12%	2%	13%	11%	4%

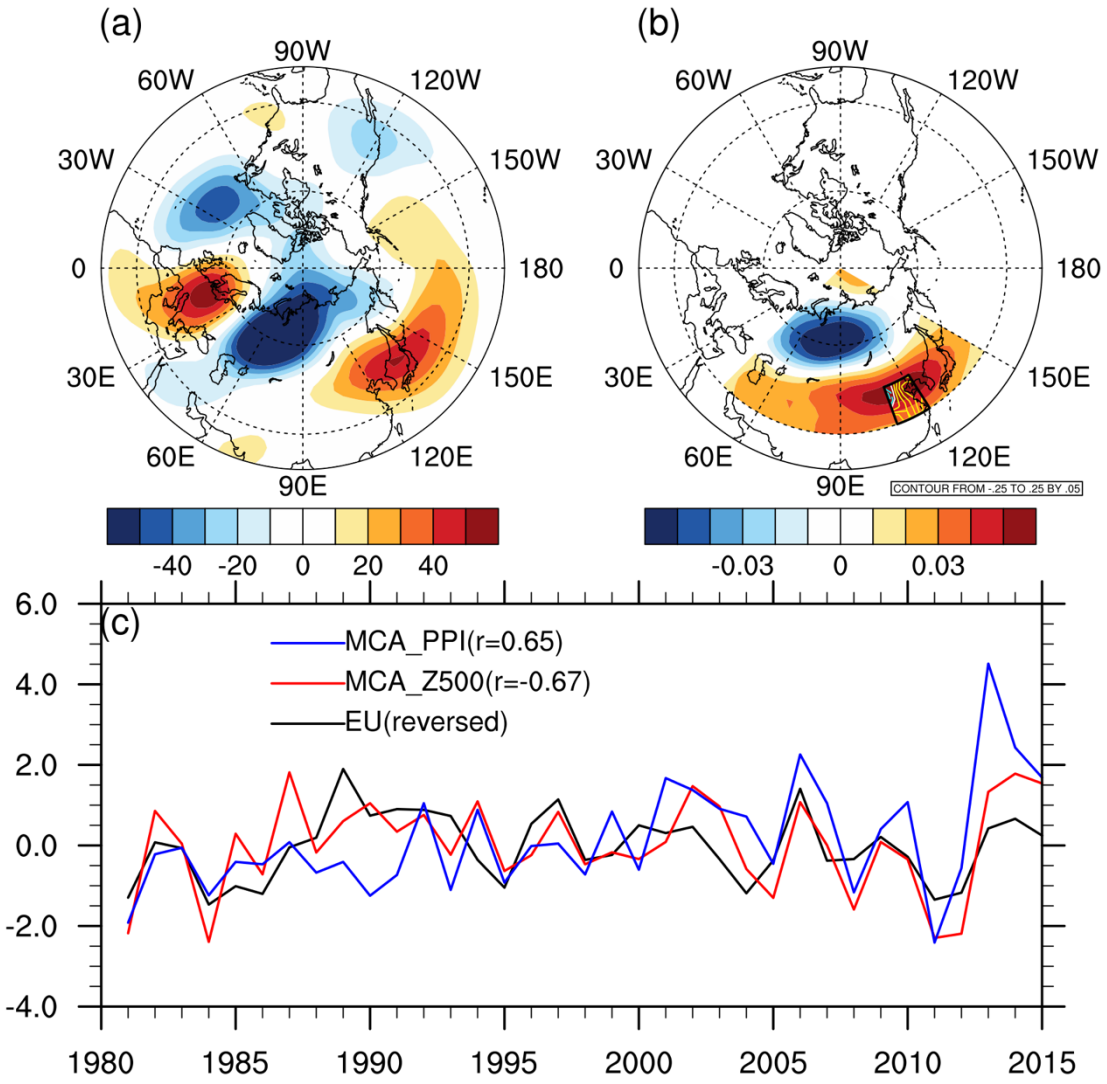

Figure S1. Comparison of the circulation patterns related with regional air stagnation over ECP based on the NCEP reanalysis data. (a) spatial distribution of the EU pattern in negative phase (shading) in the 500 hPa geopotential height field (unit: m); (b) spatial distribution of the first modes of MCA_Z500 in positive phase (shading) and MCA_PPI in positive phase (contours with interval of 0.05; the yellow solid lines denote the positive contours; the white line denotes the zero contour; the cyan dashed lines denote the negative contours); the black box denotes the ECP region (112° E to 122° E, 30° N to 41° N); (c) time series of the two circulation patterns and the MCA_PPI index in January from 1981 to 2015. The r value in the parentheses after the MCA_PPI legend is the correlation coefficient between MCA_PPI and MCA_Z500. The r value in the parentheses after the MCA_Z500 legend is the correlation coefficient between MCA_Z500 and EU. The sign of the EU index is reversed for better comparison with the MCA_Z500 index.

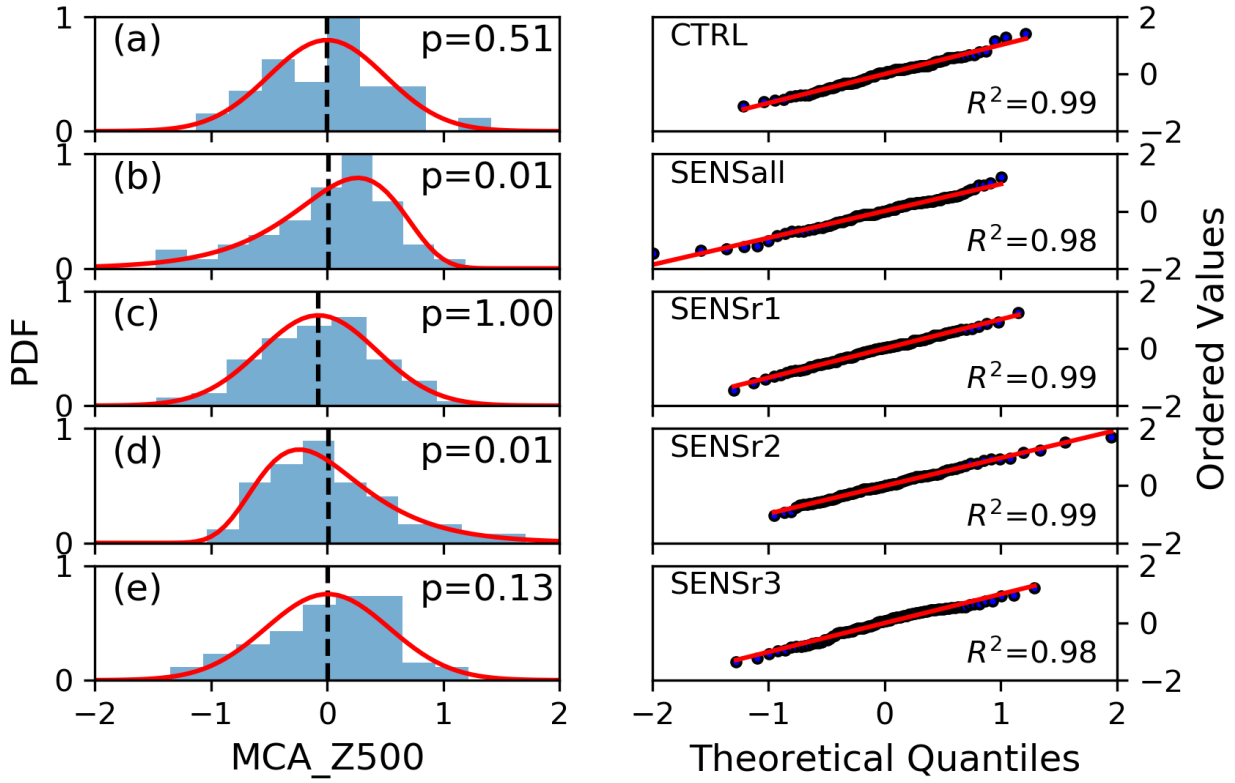

Figure S2. Evaluation of the MCA_Z500 distribution fitting in the WACCM experiments. The left panels show the comparison of the histograms and fitted PDF curves of MCA_Z500 in winter months (Dec, Jan, and Feb), and the right panels show the Q-Q plots by comparing the sample quantiles from the corresponding experiments against the theoretical ones of the distribution. The black dashed lines and p values in the left panel denote the ensemble means and the normality test results of each experiment, and the red lines and R^2 values in the right panel denote the least-squares regression fits to the quantile data and their corresponding goodness-of-fit. The statistical properties in Table S2 and the histograms of each experiment suggest (a) a normal distribution in CTRL; (b) a left-skewed distribution with "changed symmetry" in SENSall; (c) a normal distribution with "increased variability" in SENSr1; (d) a right-skewed distribution with "changed symmetry" in SENSr2; (e) a normal distribution with "increased variability" in SENSr3.

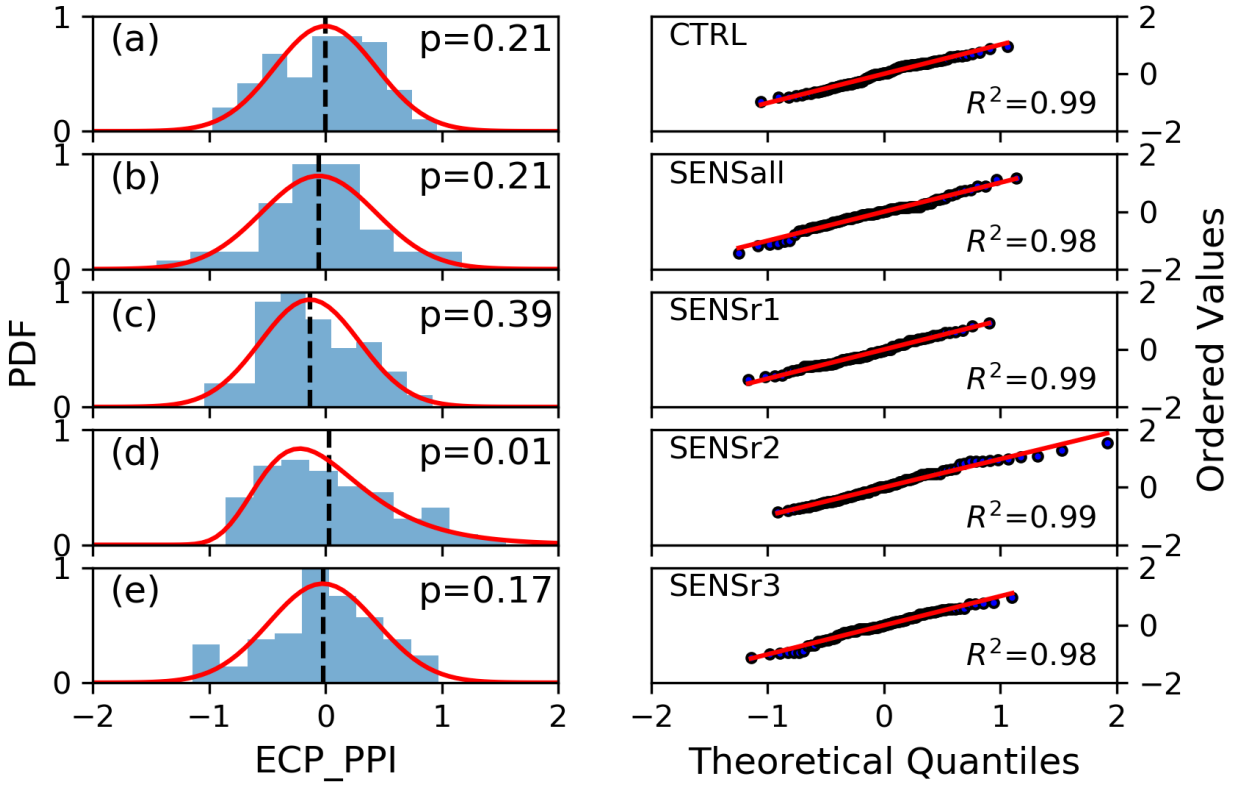

Figure S3. Evaluation of the ECP_PPI distribution fitting in the WACCM experiments. The left panels show the comparison of the histograms and fitted PDF curves of ECP_PPI in winter months (Dec, Jan, and Feb), and the right panels show the Q-Q plots by comparing the sample quantiles from the corresponding experiments against the theoretical ones of the distribution. The black dashed lines and p values in the left panel denote the ensemble means and the normality test results of each experiment, and the red lines and R^2 values in the right panel denote the least-squares regression fits to the quantile data and their corresponding goodness-of-fit. The statistical properties in Table S2 and the histograms of each experiment suggest (a) a normal distribution in CTRL; (b) a normal distribution with "increased variability" in SENSall; (c) a normal distribution with "shifted mean" in SENSr1; (d) a right-skewed distribution with "changed symmetry" in SENSr2; (e) a normal distribution with "increased variability" in SENSr3.

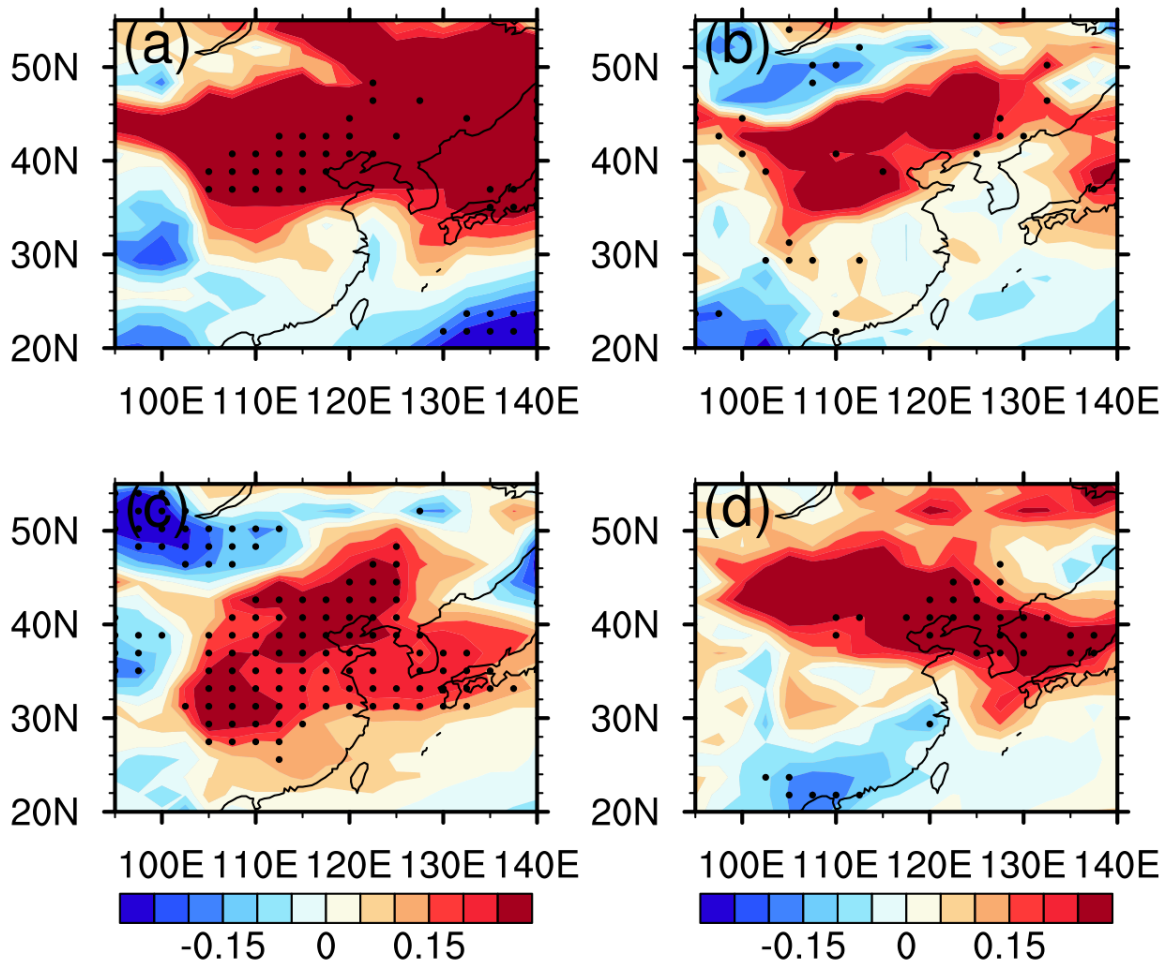

Figure S4. Spatial distributions of surface $PM_{2.5}$ concentration percentage changes (unit: 100%) in extreme members of each sensitivity experiment relative to the CTRL ensemble mean result. (a) SENSall; (b) SENSr1; (c) SENSr2; (d) SENSr3. The stipples denote the 0.05 significance level.

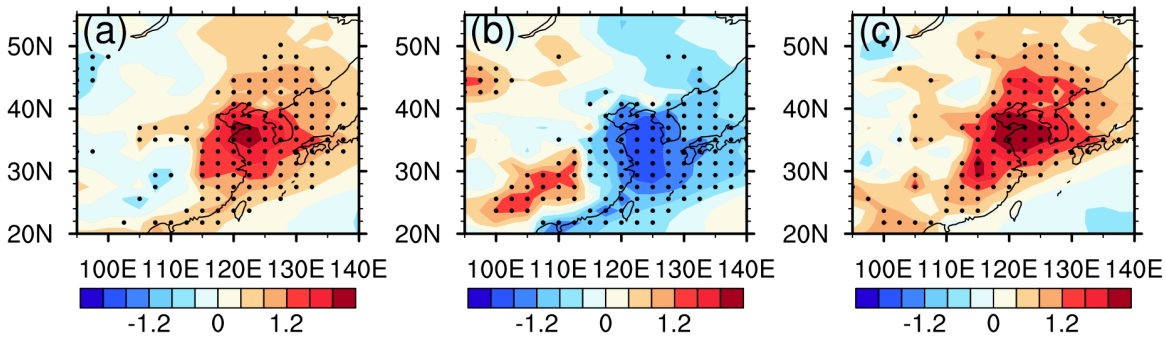

Figure S5. Spatial distributions of regional ventilation condition changes (unitless) in the SENSr2 experiment. (a) PPI differences between SENSr2 extreme members and CTRL ensemble mean; (b) WSI differences between SENSr2 extreme members and CTRL ensemble mean; (c) ATGI differences between SENSr2 extreme members and CTRL ensemble mean. The stipples denote the 0.05 significance level.

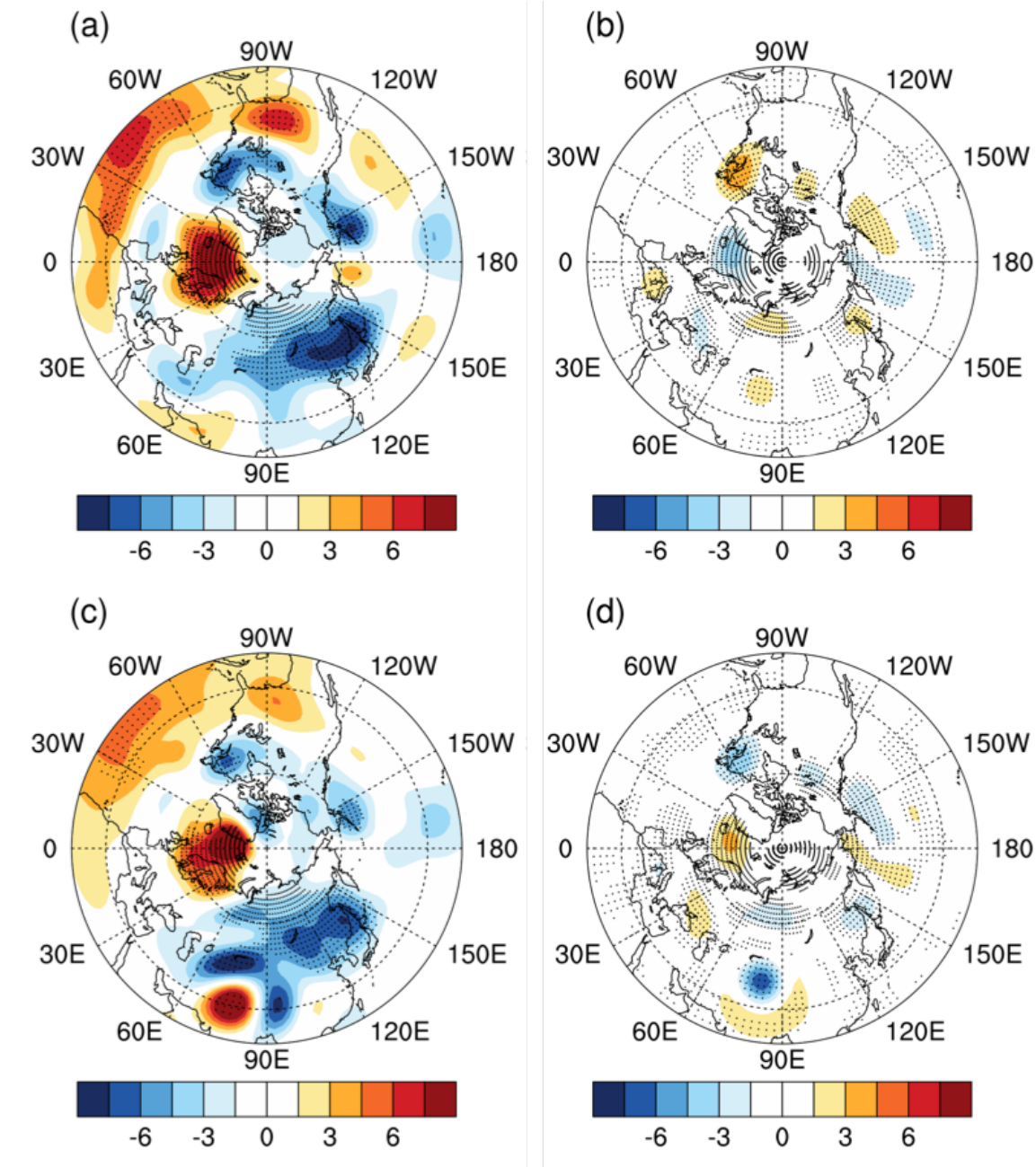

Figure S6. Comparison of geopotential height tendencies (unit: m/day) in the extreme members of WACCM SESN3 driven by (a) transient eddy vorticity forcing (Z_t^V) in the upper troposphere at 250 hPa; (b) transient eddy heat forcing (Z_t^H) at 250 hPa; (c) transient eddy vorticity forcing (Z_t^V) in the lower troposphere at 850 hPa; (d) transient eddy heat forcing (Z_t^H) at 850 hPa. The stipples denote the 0.05 significance level.

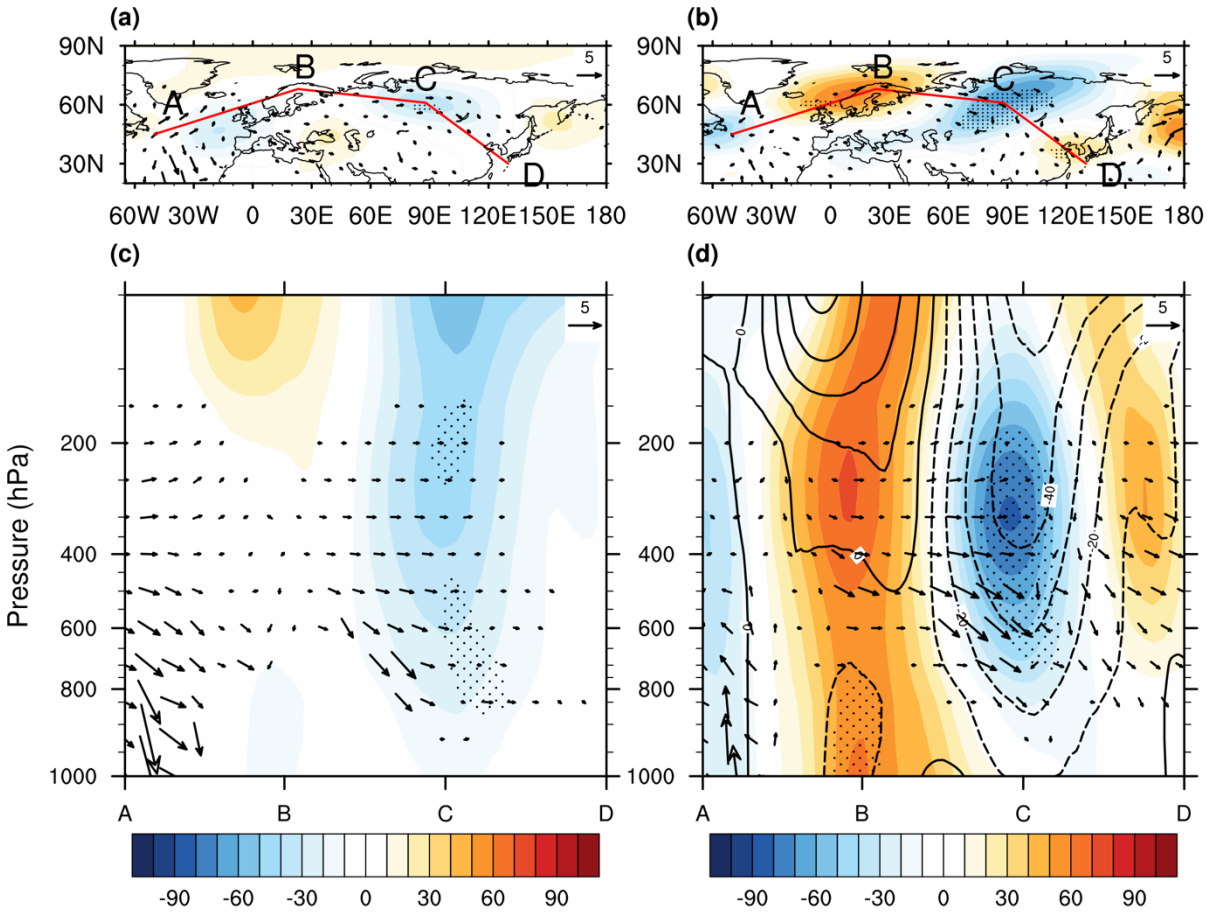

Figure S7. Comparison of anomalous atmospheric wave activity in the WACCM CTRL and SENSr2 experiments. (a) model-based ensemble mean geopotential heights at 500 hPa (color shading, m) and wave activity flux (WAF) at 250 hPa (vectors, $m^2 s^{-2}$) of the CTRL counterparts of the SENSr2 extreme members (relative to the CTRL ensemble mean); (b) same as (a) but based on the SENSr2 extreme members (relative to their CTRL counterparts); (c) model-based vertical cross section of geopotential heights (color shading, m) and WAF (vectors, $m^2 s^{-2}$) of the CTRL counterparts of the SENSr2 extreme members (relative to the CTRL ensemble mean) along the wave propagation path shown in (a); (d) same as (c) but based on the SENSr2 extreme members (relative to their CTRL counterparts); The contours denoting the anomalous geopotential heights of the CTRL counterparts in (c) are overlaid for direct comparison. Note that the vertical components of WAF in (c)-(d) were scaled up by 200 for clear illustration. The stipples denote the 0.05 significance level.

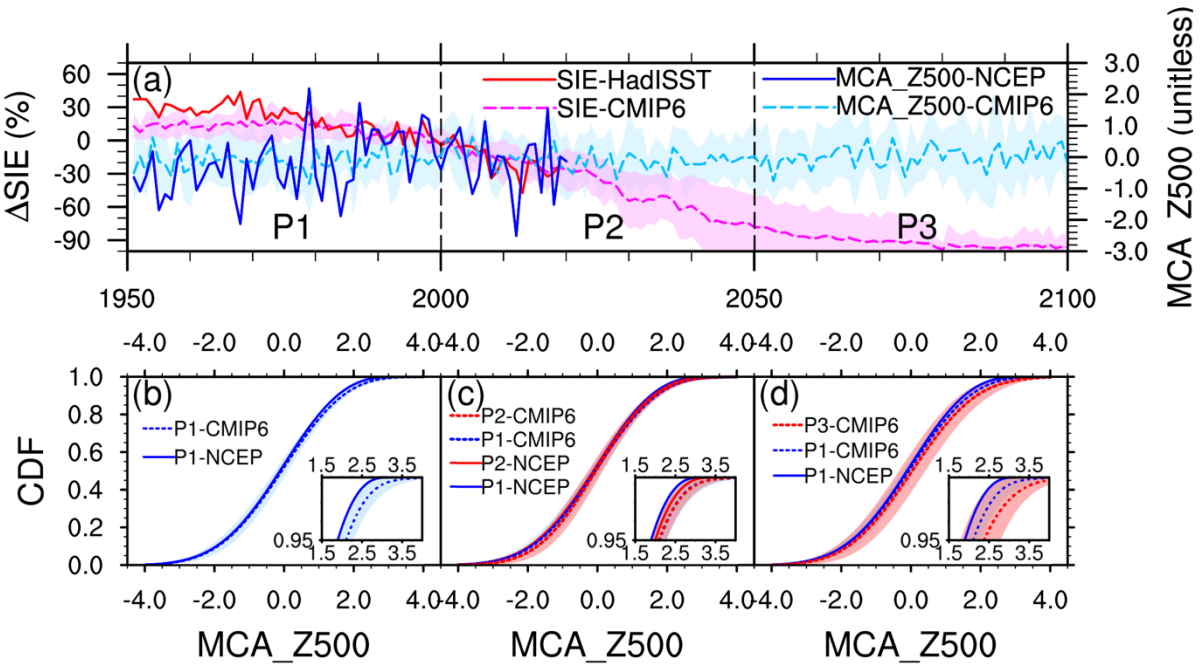

Figure S8. Historical simulations and future projections (under the SSP5-8.5 scenario) of Arctic sea ice and regional circulation in observational and reanalysis data and CMIP6 models. (a) time series of the Arctic SIE relative changes (unit: %; relative to 1981-2010) in preceding September and MCA_Z500 (unitless) in DJF of the following winter (using years of January for X-axis labeling). The solid lines denote observation- and reanalysis-based Arctic SIE and MCA_Z500 from 1950 to 2019. The dashed lines denote ensemble mean and the color shading denotes ±1 standard deviation of the 8 CMIP6 models (see Table S1 for model details) from 1950 to 2100. Note that the SIE time series were shifted forward by one year to align with the MCA_Z500 data; (b) comparison of MCA_Z500 CDF curves between the NCEP reanalysis data and the CMIP6 models in the P1 time period from 1951 to 2000. The inset denotes the distributions of positive extremes ($\geq MCA\_Z500_{\mathrm{P1}}^{95^{th}}$). The color shading denotes ±1 standard deviations in the 8 CMIP6 models; (c) Same as (b) but for the comparison between P1 and P2 (2001-2050) time periods as well as between the NCEP reanalysis data and the CMIP6 models; (d) same as (b) but for the comparison between P1 and P3 (2051-2100) time periods as well as between the NCEP reanalysis data and the CMIP6 models.

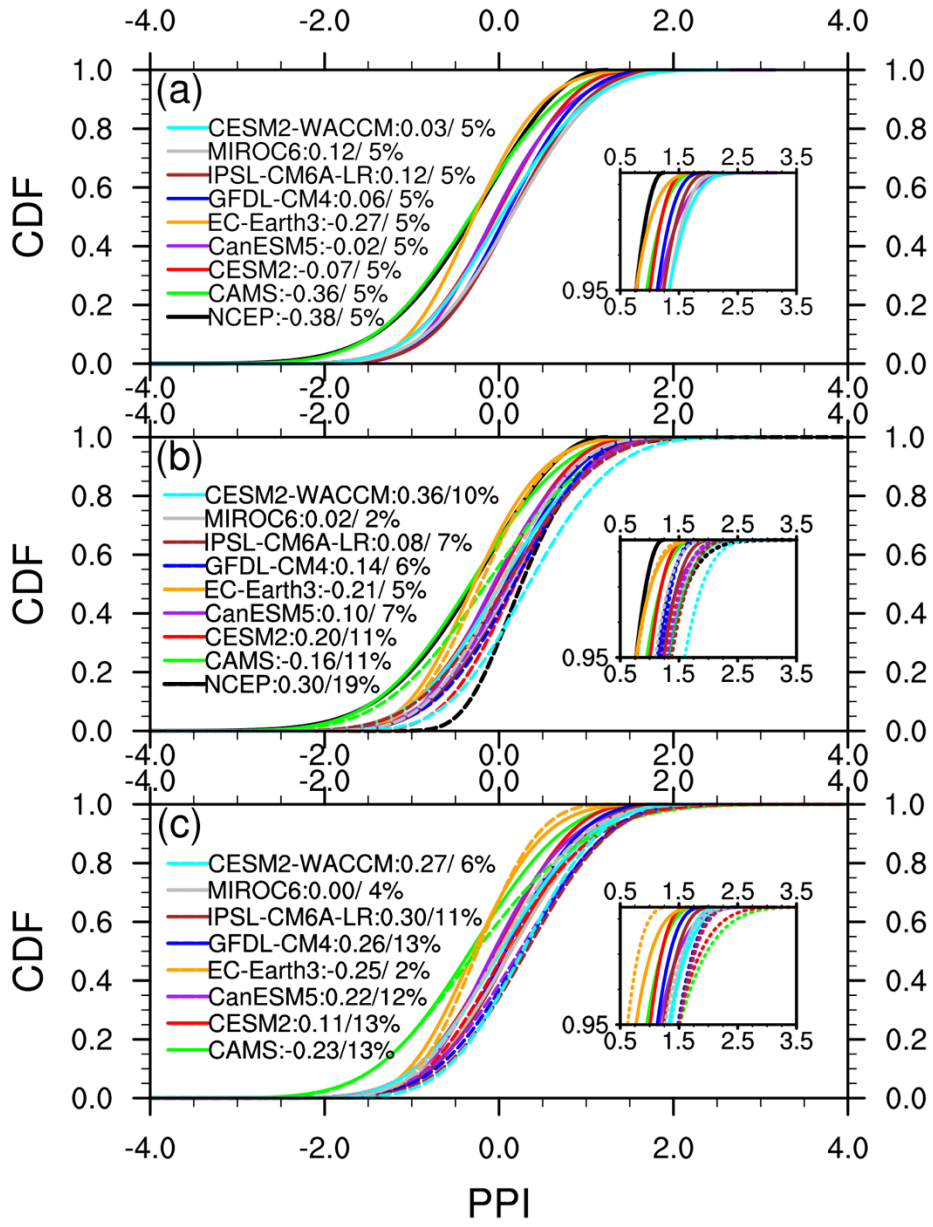

Figure S9. Historical distribution and future projections (under the SSP5-8.5 scenario) of regional air stagnation in winter (DJF) in NCEP reanalysis and CMIP6 models. (a) CDFs of historical ECP_PPI during the P1 period (1951-2000); (b) comparison of ECP_PPI CDFs between historical (solid lines) and near-term projections (dashed lines) during the P2 period (2001-2050). The NCEP ECP_PPI data in P2 are from 2001 to 2019; (c) comparison of ECP_PPI CDFs between historical (solid lines) and long-term projections (dashed lines) during the P3 period (2051-2100). In (a)-(c), the numbers and percentages after each legend name denote ensemble mean values and probabilities of positive extreme values in P1-P3, respectively.

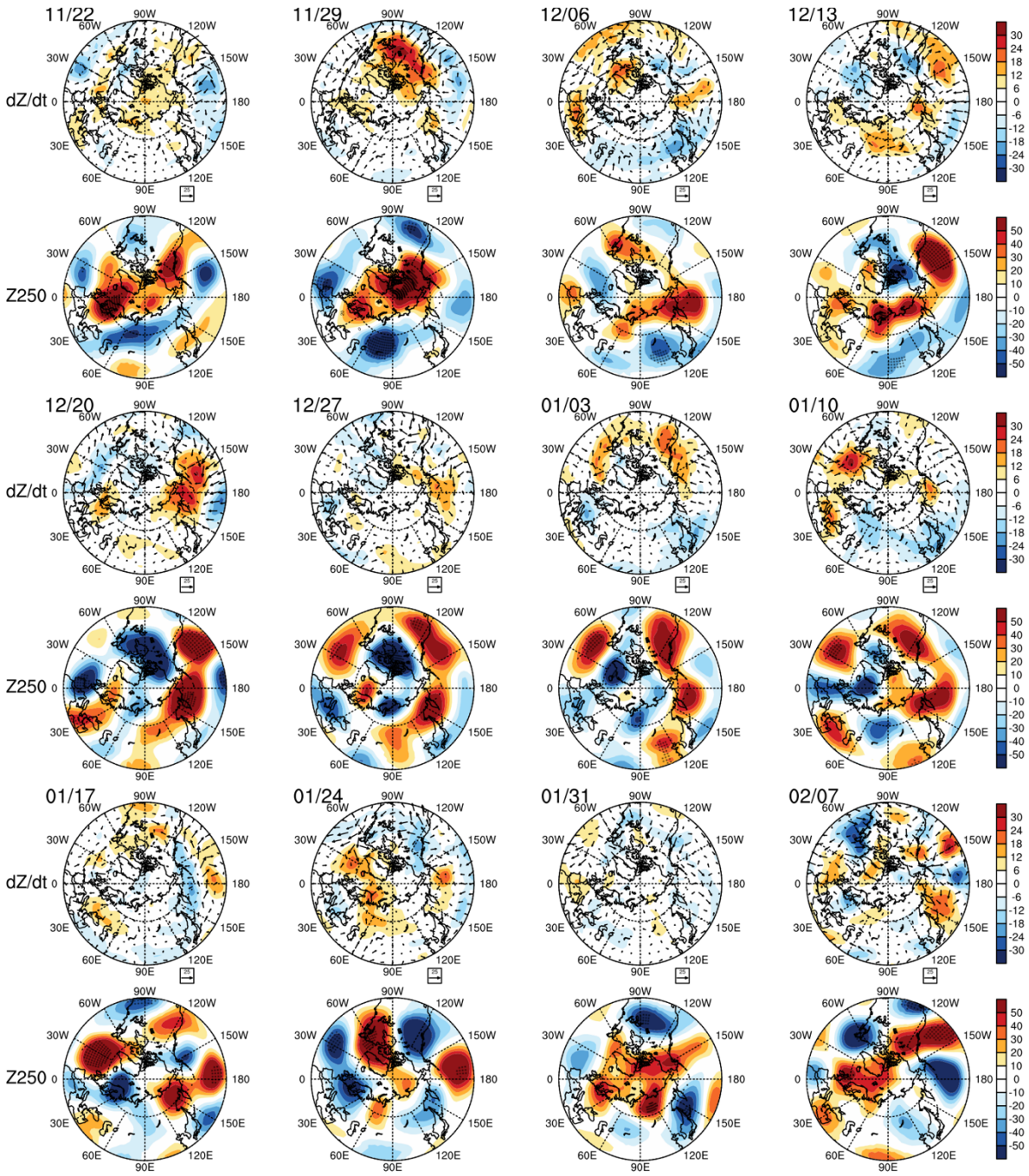

Figure S10. Weekly evolution of E vectors (unit: m^2/s^2), geopotential height tendencies (unit: m/day), and height anomalies (unit: m) at 250 hPa in SENSr2 ensemble mean. The dates on top left corners denote the first days of each week. The stipples in anomalous Z250 fields denote the 0.05 significance level.

References

Boucher, O., Denvil, S., Caubel, A., et al.: IPSL-CM6A-LR model output prepared for CMIP6 CMIP historical. ***Version 20180803***. Earth System Grid Federation. http://doi.org/10.22033/ESGF/CMIP6.5195, 2018.

Boucher, O., Denvil, S., Caubel, A., et al.: IPSL-CM6A-LR model output prepared for CMIP6 ScenarioMIP ssp585. ***Version 20190119***. Earth System Grid Federation. http://doi.org/10.22033/ESGF/CMIP6.5271, 2019.

CCCma: CCCma CanESM5 model output prepared for CMIP6 CMIP historical. ***Version 20190429***. Earth System Grid Federation. http://cera-www.dkrz.de/WDCC/meta/CMIP6/CMIP6.CMIP.CCCma.CanESM5.historical, 2018.

CCCma: CCCma CanESM5 model output prepared for CMIP6 ScenarioMIP ssp585. ***Version 20190429***. Earth System Grid Federation. http://cera-www.dkrz.de/WDCC/meta/CMIP6/CMIP6.ScenarioMIP.CCCma.CanESM5.ssp585, 2018.

Danabasoglu, G., Lawrence, D., Lindsay, K., et al.: NCAR CESM2 model output prepared for CMIP6 CMIP historical. ***Version 20190308***. Earth System Grid Federation. http://doi.org/10.22033/ESGF/CMIP6.7627, 2019.

Danabasoglu, Gokhan: NCAR CESM2 model output prepared for CMIP6 ScenarioMIP ssp585. ***Version 20190730***. Earth System Grid Federation. http://doi.org/10.22033/ESGF/CMIP6.7768, 2019.

Danabasoglu, Gokhan: NCAR CESM2-WACCM model output prepared for CMIP6 CMIP historical. ***Version 20190227***. Earth System Grid Federation. http://doi.org/10.22033/ESGF/CMIP6.10071, 2019.

Danabasoglu, Gokhan: NCAR CESM2-WACCM model output prepared for CMIP6 ScenarioMIP ssp585. ***Version 20190815***. Earth System Grid Federation. http://doi.org/10.22033/ESGF/CMIP6.10115, 2019.

EC-Earth Consortium (EC-Earth): EC-Earth-Consortium EC-Earth3-Veg model output prepared for CMIP6 CMIP historical. ***Version 20190605***. Earth System Grid Federation. http://doi.org/10.22033/ESGF/CMIP6.4706, 2019.

EC-Earth Consortium (EC-Earth): EC-Earth-Consortium EC-Earth3-Veg model output prepared for CMIP6 ScenarioMIP ssp585. ***Version 20190629***. Earth System Grid Federation. http://doi.org/10.22033/ESGF/CMIP6.4914, 2019.

Guo, H., John, J.G., Blanton, C., et al.: NOAA-GFDL GFDL-CM4 model output prepared for CMIP6 CMIP historical. ***Version 20180701***. Earth System Grid Federation. http://doi.org/10.22033/ESGF/CMIP6.8594, 2018.

Guo, H., John, J.G., Blanton, C., et al.: NOAA-GFDL GFDL-CM4 model output prepared for CMIP6 ScenarioMIP ssp585. ***Version 20180701***. Earth System Grid Federation. http://doi.org/10.22033/ESGF/CMIP6.9268, 2018.

Rong, X.: CAMS CAMS_CSM1.0 model output prepared for CMIP6 CMIP historical. ***Version 20190708***. Earth System Grid Federation. http://doi.org/10.22033/ESGF/CMIP6.9754, 2019.

Rong, X.: CAMS CAMS_CSM1.0 model output prepared for CMIP6 ScenarioMIP ssp585. ***Version 20190708***. Earth System Grid Federation. http://doi.org/10.22033/ESGF/CMIP6.11052, 2019.

Shiogama, H., Abe, M., Tatebe, H., et al.: MIROC MIROC6 model output prepared for CMIP6 ScenarioMIP ssp585. ***Version 20190627***. Earth System Grid Federation. http://doi.org/10.22033/ESGF/CMIP6.5771, 2019

Tatebe, H. and Watanabe, M.: MIROC MIROC6 model output prepared for CMIP6 CMIP historical. ***Version 20181212***. Earth System Grid Federation. http://doi.org/10.22033/ESGF/CMIP6.5603, 2018